HHS Public Access
Author manuscript
Proc IEEE Int Symp Biomed Imaging. Author manuscript; available in PMC 2019 February 15.

Published in final edited form as:
Proc IEEE Int Symp Biomed Imaging. 2011 ; 2011: 1520–1523. doi:10.1109/ISBI.2011.5872690.

REGISTRATION OF BRAIN RESECTION MRI WITH INTENSITY AND LOCATION PRIORS

Nicha Chitphakdithai[1], **Kenneth P. Vives**[2], and **James S. Duncan**[1,3,4]

[1]Department of Biomedical Engineering, Yale University, New Haven, CT, USA

[2]Department of Neurosurgery, Yale School of Medicine, New Haven, CT, USA

[3]Department of Diagnostic Radiology, Yale University, New Haven, CT, USA

[4]Departments of Electrical Engineering, Yale University, New Haven, CT, USA

Abstract

Images with missing correspondences are difficult to align using standard registration methods due to the assumption that the same features appear in both images. To address this problem in brain resection images, we have recently proposed an algorithm in which the registration process is aided by an indicator map that is simultaneously estimated to distinguish between missing and valid tissue. We now extend our method to include both intensity and location information for the missing data. We introduce a prior on the indicator map using a Markov random field (MRF) framework to incorporate map smoothness and spatial knowledge of the missing correspondences. The parameters for the indicator map prior are automatically estimated along with the transformation and indicator map. The new method improves both segmentation and registration accuracy as demonstrated using synthetic and real patient data.

Keywords

Image Registration; Missing Correspondences; MAP Estimation; EM Algorithm; MRF Prior

1. INTRODUCTION

Medical image registration techniques generally assume a one-to-one correspondence between features in the images to be registered, using one similarity metric for the whole image to define how closely the pair matches. However, when the images are missing correspondences, such as due to resection or tumor treatment, the one-to-one correspondence assumption is violated. Standard registration methods will likely cause misalignment of the images, especially near regions with missing data, which are usually the places we are most interested in matching.

Few previously proposed methods have targeted image registration with missing correspondences. Biomechanical models along with deformable registration methods have been used to align brain tumor images to a normal brain atlas [1]. A more generally applicable method was introduced in [2], in which an explicit model was used for matching and missing data, but the estimation for the partial data considered only an image similarity term. A point-based non-rigid registration algorithm for aligning pre- and intra-operative tumor resection images was presented in [3].

In addition, we have recently proposed an approach in which the voxel-based registration is assisted by an indicator map to segment the different correspondence regions. The general joint registration and segmentation framework solved using the expectation maximization (EM) algorithm is based on [4]. We first introduced the registration and indicator map estimation (RIME) approach in [5], and included only a postresection intensity prior in [6] for alignment of preoperative and postresection brain images of epilepsy patients. While the previous method greatly lowered registration errors, we saw the indicator map estimation still needed improvement. Under the joint estimation framework, the image alignment should benefit from an improved indicator map estimate. Also, an accurate estimate for the valid tissue region is important so that any comparisons made between the registered images, such as in fMRI analysis, are only performed on voxels with valid correspondences.

Thus, here we extend the approach to include an MRF-based prior on the indicator map to smooth the estimate and incorporate location information for the missing region. For our example case of pre- and post-resection brain alignment, we use an atlas to store segmented brain regions. The location information will then be provided to our algorithm by choosing the atlas label that best corresponds to the resection volume. With patient data, the resection location will likely already be noted, but a user may identify the proper atlas label with a quick visual inspection of the image. We automatically tune the parameters for the indicator map prior model under the EM framework. We compare the new approach with other methods using synthetic images as well as patient data.

2. METHODS

2.1. Registration and Indicator Map Estimation

The basic framework for the joint registration and indicator map estimation problem is described in [6]. We briefly review the setup and introduce the new algorithmic steps here.

Our goal is to find the registration parameters R which align voxel $\mathbf{x}$ in reference image S with voxel $R(\mathbf{x})$ in moving image T. We include a “hidden” indicator map I with a set of labels to segment different correspondence regions; for example, in the case of aligning preoperative and postresection brain data, we may have a label for valid tissue and a label for the resection. Under a maximum a posteriori (MAP) framework, we search for

$$\hat{R} = \arg\max_{R} \log \sum_{I} p(R, I \mid S, T) . \quad (1)$$

We apply the EM algorithm to solve the problem. The registration parameters are updated during the M-step by maximizing the expectation of the posterior:

$$R^{k+1} = \arg\max_R E_{I \mid S, T, R^k}[\log p(T \mid S, I, R) + \log p(S \mid I, R) + \log p(I \mid R) + \log p(R)]. \quad (2)$$

We rewrite the expectation as a sum over all voxels **x** in the reference image S and all possible labels l in the indicator map I. In addition, we assume that given the indicator map, the reference image does not depend on the transformation. Finally, we assume that the prior on the indicator map does not depend on the registration parameters. Dropping terms that do not depend on R, (2) simplifies to

$$R^{k+1} = \arg\max_R \left[\sum_{\mathbf{x}} \sum_l (p(I(\mathbf{x}) = l \mid S, T, R^k) \cdot \log p(T(R(\mathbf{x})) \mid S, I(\mathbf{x}) = l, R)) + \log p(R) \right]. \quad (3)$$

The indicator map estimation is updated in the E-step. Using Bayes rule and simplifying, we have

$$p(I(\mathbf{x}) = l \mid S, T, R^k) = \frac{p\left(T\left(R^k(\mathbf{x})\right) \mid S, I(\mathbf{x}) = l, R^k\right) p(S(\mathbf{x}) \mid I(\mathbf{x}) = l) p(I(\mathbf{x}) = l)}{\sum_{l'} p\left(T\left(R^k(\mathbf{x})\right) \mid S, I(\mathbf{x}) = l', R^k\right) p(S(\mathbf{x}) \mid I(\mathbf{x}) = l') p(I(\mathbf{x}) = l')}. \quad (4)$$

When the EM algorithm converges, we estimate the final indicator map as $\hat{I}(\mathbf{x}) = \arg\max_l p\left(I(\mathbf{x}) = l \mid S, T, \hat{R}\right)$.

2.2. Probability Model Instantiation

In the following, we use 3 labels to distinguish the missing correspondence, valid correspondence, and background regions. The probability models used for the matching term $p(T(R(\mathbf{x})) \mid S, I(\mathbf{x}) = l, R)$, the reference image intensity prior $p(S(\mathbf{x}) \mid I(\mathbf{x}) = l)$, and the transformation prior $p(R)$ are similar to those presented in [6]. Briefly, for the similarity term, given a different indicator value at a voxel, we use a different probability distribution depending on how we expect the images to match. Similarly for the intensity prior, we use a different distribution to describe the reference image intensities given an indicator map label. The parameters for the intensity prior for missing correspondences are estimated using training data. For the transformation model, we choose free form deformations (FFDs) based on uniform cubic B-splines; the transformation prior then constrains the B-spline control points.

In this work, we focus on the incorporation of the indicator map prior. To start, we impose an MRF onto the indicator map. We can then model the prior probability of the indicator map by a Gibbs distribution [7],

$$p(I) = \frac{1}{Z} exp\left[-\beta \sum_{c} V_c(I)\right], \quad (5)$$

where Z is a normalizing constant and V_c is the potential function for clique c. To make this calculation tractable, we use the mean field theory (for a brief review, see [8]) to approximate (5) as

$$p(I) \approx \prod_{\mathbf{x}} \frac{1}{Z'_{\mathbf{x}}(\beta)} exp\left[-\left(\beta \sum_{c} V'_c(I(\mathbf{x}), \bar{I})\right)\right], \quad (6)$$

where $Z'_{\mathbf{x}}(\beta)$ is a normalizing constant that depends on x and β, and the new potential V'_c is a function of the current mean field $\bar{I}$. We approximate $\bar{I}$ with the indicator map estimate for the current iteration k of the EM algorithm, $I^k = \arg\max_{l} p(I(\mathbf{x}) = l \mid S, T, R^k)$. Considering cliques of size 1 and 2, the prior probability of an indicator map voxel taking on a certain label can be written as

$$p(I(\mathbf{x}) = l \mid \beta_L, \beta_S) \approx \frac{1}{Z'_{\mathbf{x}}(\beta_L, \beta_S)} exp\Big[\beta_L V'_L\big(l, I^A(\mathbf{x})\big) \quad (7)$$
$$+ \beta_S \sum_{\mathbf{n} \in \mathcal{N}(\mathbf{x})} V'_S\big(l, I^k(\mathbf{n})\big)\Big].$$

The location prior is encoded in the unary potential V'_L, which depends on an atlas I^A. In this work, we set $V'_L\big(l, I^A(\mathbf{x})\big)$ to be the probability that the map at voxel $\mathbf{x}$ takes on the label l as given by the probabilistic atlas. For the registration of pre- and post-resection brain images, the approximate spatial location (e.g., left temporal lobe) of the resection is known. For the label l corresponding to the missing region, the user chooses which of the possible atlas regions best corresponds to the resection location. The location prior will aid estimation of both the resected and valid correspondence regions. This will be especially helpful for CSF voxels, which are likely to be mislabled since they have similar intensity to resection voxels.

The map smoothing prior is encoded in the binary potential V'_S, which depends on the values of the neighbors $\mathcal{N}(\mathbf{x})$ of $\mathbf{x}$ in the current indicator map estimate I^k. We employ a Potts model, setting $V_S'\left(l, I^k(\mathbf{n})\right) = \delta\left(l, I^k(\mathbf{n})\right)$. The smoothing prior will help eliminate small mislabeled regions.

Note that the prior probability in (7) depends on the parameters β_L and β_S, which determine the influence of the location and smoothing priors, respectively. Rather than set these parameters, we simultaneously solve for them in the EM algorithm; now in the M-step, we not only solve for (3), but we also look for

$$\beta_L^{k+1}, \beta_S^{k+1} = \underset{\beta_L, \beta_S}{\arg\max} \sum_{\mathbf{x}} \sum_{l} p(I(\mathbf{x}) = l \mid S, T, R^k) \cdot \left[\log p(I(\mathbf{x}) = l \mid \beta_L, \beta_S) + \log p\left(\beta_L, \beta_S\right)\right]. \quad (8)$$

We assume β_L and β_S are independent and assign a normal distribution with small mean on each parameter. This will help constrain the parameters so that the indicator map estimation does not become overly dependent on the prior.

3. RESULTS

For the experiments, we registered image pairs using 4 algorithms: a standard non-rigid registration (SNRR) method based on [9], implemented in [10]; a robust similarity metric registration (RSR) method as described in [6], which reduces the influence of outliers based on the data term; our recently presented registration and indicator map estimation method with only an intensity prior (RIME-int) in [6]; and our new approach which incorporates an indicator map prior (RIME-imp). Note that all algorithms use a voxel intensity-based similarity measure and a FFD transformation model with the same control point spacings for a fair comparison.

3.1. Synthetic Data

We tested the methods on 11 synthetic 256×256 2D pre- and post-operative brain image pairs with “resections” in the upper or lower right of the image. The preoperative brain was warped using a known displacement field to create the postresection image. A probabilistic atlas for the valid tissue region was created using the preoperative images. Two regions were added for the front and back left hemispheres of the brain.

The maximum, mean, and standard deviation of the errors for pixels in the postresection image with a valid correspondence in the preoperative brain was calculated for each result. The average error measures for each registration method are shown in the bar graph in Fig. 1. The proposed RIME-imp method produced the smallest errors. Paired one-tailed t-tests were performed between errors from RIME-imp and the other methods. As noted in Fig. 1, most of the reduced error values for RIME-imp were statistically significant ($p < 0.05$).

Examples of the estimated valid correspondence region produced by the RIME-int and RIME-imp methods are shown in Figs. 2(a) and 2(b), respectively. We used the dice coefficient to measure the overlap between true and estimated valid correspondence voxels.

RIME-int resulted in an average dice coefficient of 0.98, while RIME-imp produced a significantly improved average overlap of 0.99 ($p = 0.0001$).

3.2. Patient Data

The registration algorithms were run on 6 pairs of T1-weighted pre- and post-resection brain MRI. They were first skull-stripped and affinely registered to the standard MNI brain, resulting in images with size 181×217×181 and an isotropic voxel resolution of 1.0mm. For the location prior, we created a custom atlas with 19 labels based on the MNI atlas. We divided the left and right hemispheres of each region in the original atlas and added a label for the entire brain for the possible valid tissue region.

Figure 3 shows example results for a patient with a right frontal lobe resection. A close up of a slice from the post- and pre-resection images is shown in Figs. 3(a) and 3(b), respectively. SNRR matched the background to the large resection, resulting in misalignment of several structures as seen in Fig. 3(c). RSR in Fig. 3(d) showed great improvement, but the gyrus along the blue line in the postresection brain in Fig. 3(a) was still misaligned. RIME-int and RIME-imp results in Figs. 3(e) and 3(f) showed proper alignment of the gyrus.

To quantitatively evaluate the results, we calculated the root mean squared error (RMSE) of intensities between pixels with a valid correspondence in each registered image pair. RIME-imp produced the lowest RMSE and performed significantly better than all other methods ($p < 0.05$).

Finally, we calculated the dice coefficient for the overlap between true and valid tissue regions for the RIME methods. The average dice coefficient for RIME-int was 0.92, while RIME-imp significantly increased the measure to 0.96 ($p < 0.05$). The improved indicator map estimate using RIME-imp is illustrated in Fig. 4 for a left temporal lobe resection case. Note that RIME-imp correctly labels many of the mislabled CSF voxels in the RIME-int estimate.

4. CONCLUSIONS

We have presented a registration method to handle missing correspondences, in which the registration is aided by the simultaneous estimation of an indicator map to segment the different correspondence regions. Under a MAP framework, we incorporated an image intensity prior model as well as an MRF-based indicator map prior. The new prior improved the segmentation estimate by including known location information for the valid and missing regions and enforcing map smoothness. This resulted in higher registration accuracy, as demonstrated on synthetic and real brain resection images.

In future work, we will explore increasing the number of labels in the indicator map. We propose that adding a label for the CSF, which has similar intensity to the resected region in T1-weighted MRI, will improve the indicator map estimation and thus improve the registration result. We also plan to adapt the general framework to other registration problems with missing correspondences, such as the alignment of longitudinal brain tumor images.

Acknowledgments

This work was supported by NIH R01 EB000473–09.

5. REFERENCES

[1]. Mohamed A, Zacharaki EI, Shen D, and Davatzikos C, "Deformable registration of brain tumor images via a statistical model of tumor-induced deformation," Med Image Anal, vol. 10, no. 5, pp. 752–763, 10 2006. [PubMed: 16860588]

[2]. Periaswamy S and Farid H, "Medical image registration with partial data," Med Image Anal, vol. 10, pp. 452–464, 2006. [PubMed: 15979375]

[3]. Liu Y, Yao C, Zhou L, and Chrisochoides N, "A point based non-rigid registration for tumor resection using imri," in 2010 7th IEEE Int'l Symposium on Biomedical Imaging: From Nano to Macro, 2010, pp. 1217 – 1220.

[4]. Pohl KM, Fisher J, Grimson WEL, Kikinis R, and Wells WM, "A bayesian model for joint segmentation and registration," NeuroImage, vol. 31, no. 1, pp. 228–239, 2006. [PubMed: 16466677]

[5]. Chitphakdithai N and Duncan JS, "Pairwise registration of images with missing correspondences due to resection," in 7th IEEE Int'l Symposium on Biomedical Imaging: From Nano to Macro, 2010, pp. 1025 –1028.

[6]. Chitphakdithai N and Duncan JS, "Non-rigid registration with missing correspondences in preoperative and postresection brain images," in MICCAI 2010, Jiang Josien P.W. Pluim Tianzi, Navab Nassir and Viergever Max A., Eds. 2010, vol. 6361, pp. 367–374, Springer, Heidelberg.

[7]. Besag J, "Spatial interaction and the statistical analysis of lattice systems," J Roy Statist Soc, vol. 36, no. 2, pp. 192–236, 1974.

[8]. Zhang J, "The mean field theory in em procedures for blind markov random field image restoration," IEEE Trans Image Proc, vol. 2, pp. 27–40, 1 1993.

[9]. Rueckert D, Sonoda LI, Hayes C, Hill DL, Leach MO, and Hawkes DJ, "Nonrigid registration using free-form deformations: application to breast mr images," IEEE Trans Med Imaging, vol. 18, no. 8, pp. 712–721, 1999. [PubMed: 10534053]

[10]. Papademetris X, Jackowski M, Rajeevan N, Okuda H, Constable RT, and H Staib L, *BioImage Suite: An integrated medical image analysis suite*, Section of Bioimaging Sciences, Dept. of Diagnostic Radiology, Yale School of Medicine, http://www.bioimagesuite.org .

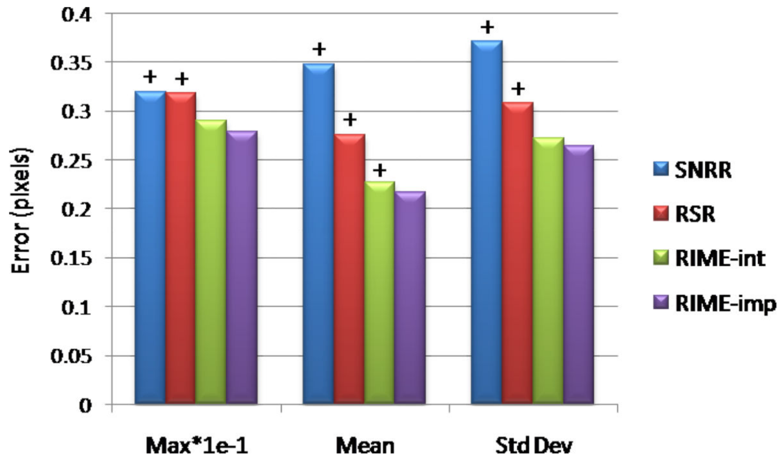

Fig. 1:

Average displacement errors (in voxels) for each registration method. Max error is scaled for plot visualization. The + above a bar denotes that the error value for that method was significantly higher compared to RIME-imp ($p < 0.05$).

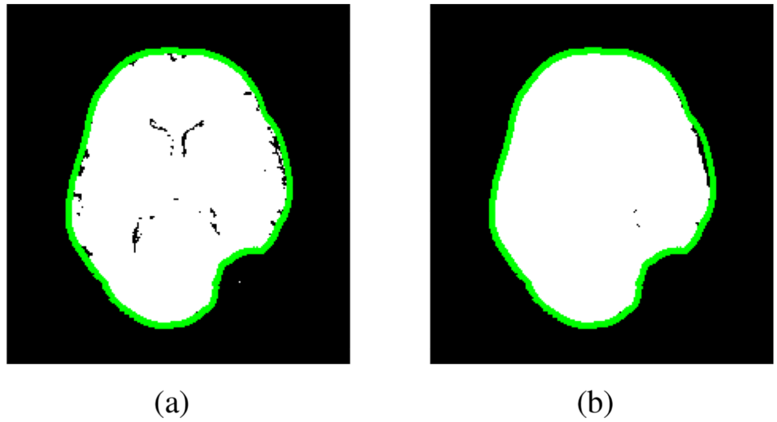

Fig. 2:
Estimated valid correspondence region for a synthetic image using (a) RIME-int and (b) RIME-imp, with true valid correspondence region outlined in green.

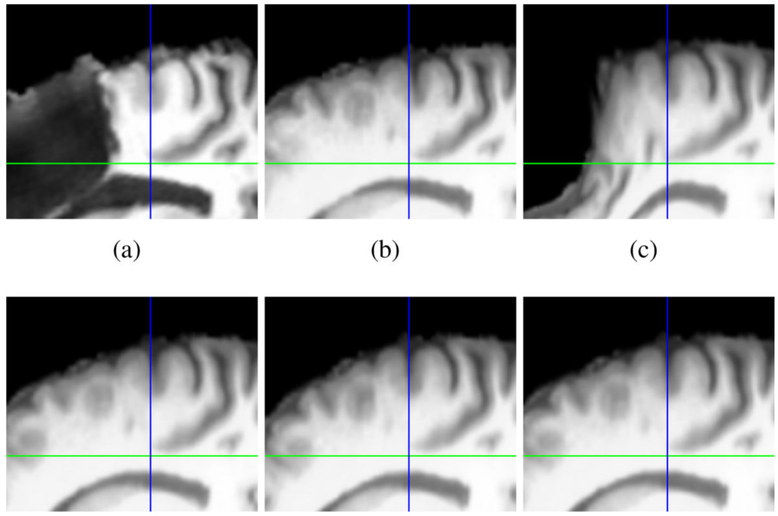

(a) (b) (c)

(d) (e) (f)

Fig. 3:

Example using real data. Close up of (a) post-resection, (b) affinely aligned pre-resection, and registration results using (c) SNRR, (d) RSR, (e) RIME-int, and (f) RIME-imp. Note alignment of the gyrus along the blue line.

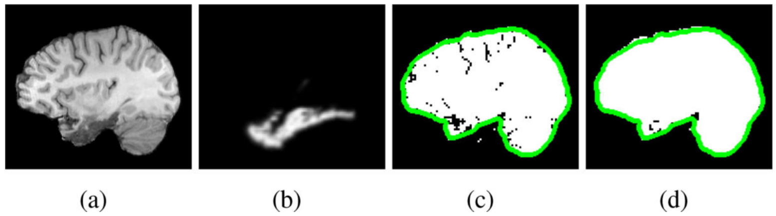

Fig. 4:
(a) Patient with left temporal lobe resection. (b) Corresponding slice from atlas for location prior for missing region. Estimated valid correspondence region using (c) RIME-int and (d) RIME-imp, with true valid correspondence region outlined in green.